Electronic Supplementary Material (ESI) for Journal of Materials Chemistry A.

Electronic Supplementary Information

MOF-Derived Conductive Carbon Nitrides for Separator-Modified Li–S Batteries and Flexible Supercapacitors

Jingsheng Cai‡[a], Yingze Song‡[a], Xiang Chen‡[b], Zhongti Sun[a], Yuyang Yi[a], Jingyu Sun[a], and Qiang Zhang*[b]*

[a]College of Energy, Soochow Institute for Energy and Materials InnovationS, Key Laboratory of Advanced Carbon Materials and Wearable Energy Technologies of Jiangsu Province Soochow University, Suzhou 215006, P. R. China

[b]Beijing Key Laboratory of Green Chemical Reaction Engineering and Technology, Department of Chemical Engineering, Tsinghua University, Beijing 100084, P. R. China

‡ These authors contributed equally to this work.

*Corresponding authors: sunjy86@suda.edu.cn (J. Y. Sun); zhang-qiang@mails.tsinghua.edu.cn (Q. Zhang)

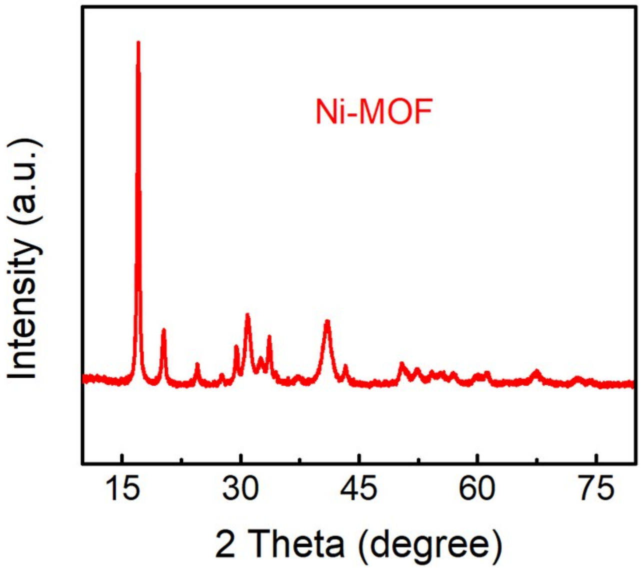

Fig. S1 XRD of the Ni-based MOF precursor.

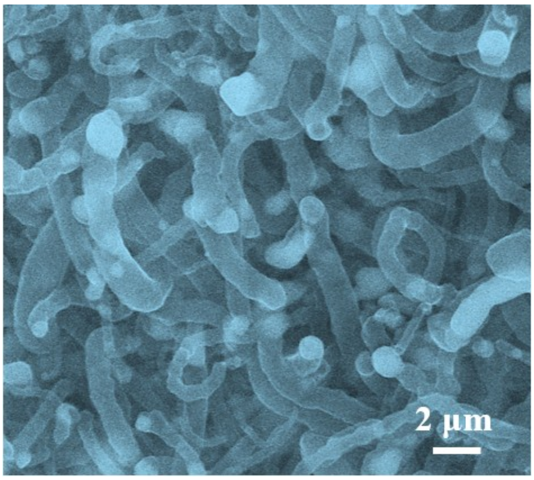

Fig. S2 SEM image of the incomplete generated c-CN, showing that Ni serves as the catalytic center for the generation of c-CN.

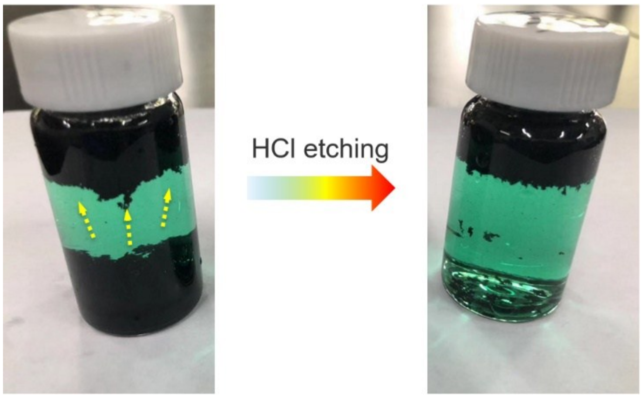

Fig. S3 Digital photographs showing the preparation of c-CN with hydrophobic nature during and after the etching process.

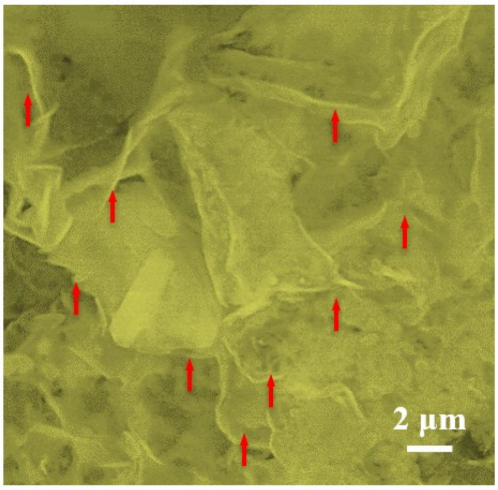

Fig. S4 SEM image of g-C_3N_4 nanosheets prepared from the conventional thermal condensation of urea. The edges of nanosheets are indicated by red arrows.

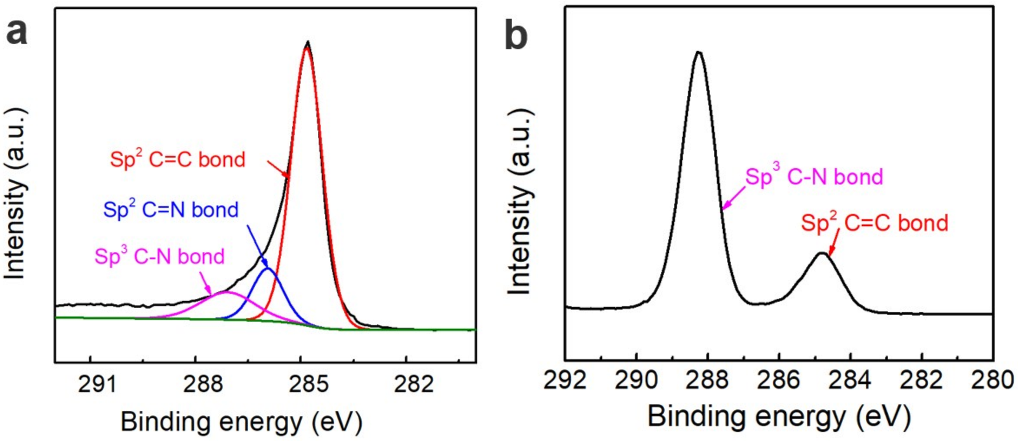

Fig. S5 XPS high-resolution C 1s spectrum of (a) c-CN and (b) g-C_3N_4.

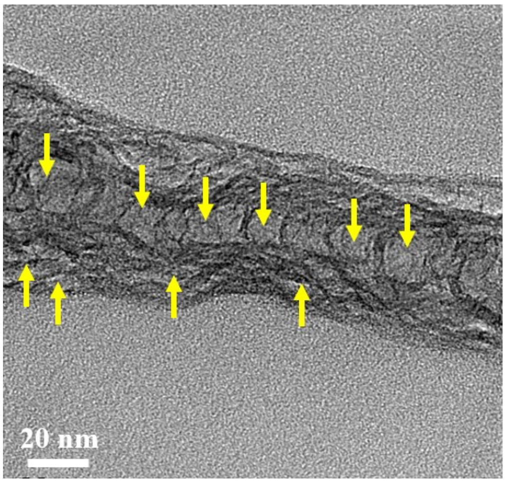

Fig. S6 TEM image of c-CN, demonstrating porosities and morphological defects.

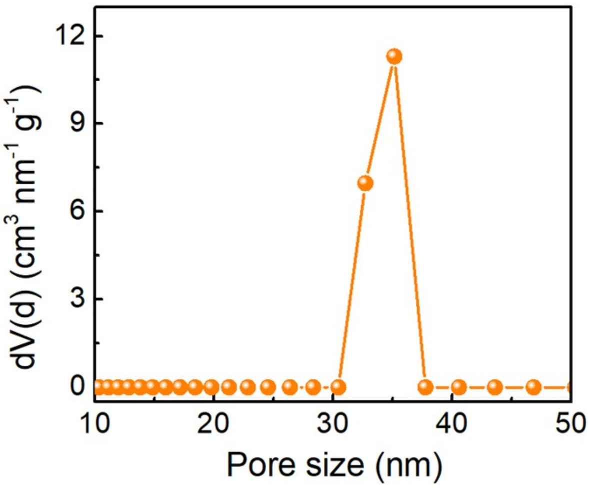

Fig. S7 The pore size distribution of c-CN.

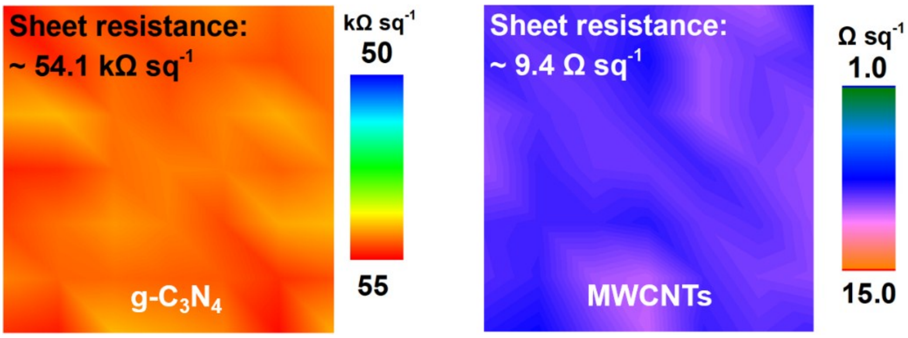

Fig. S8 Sheet resistance map of the g-C_3N_4 and MWCNTs films.

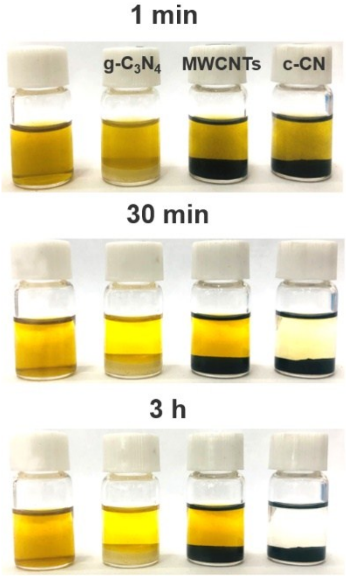

Fig. S9 Digital photograph showing the Li_2S_6 adsorption tests of g-C_3N_4, MWCNTs, and c-CN.

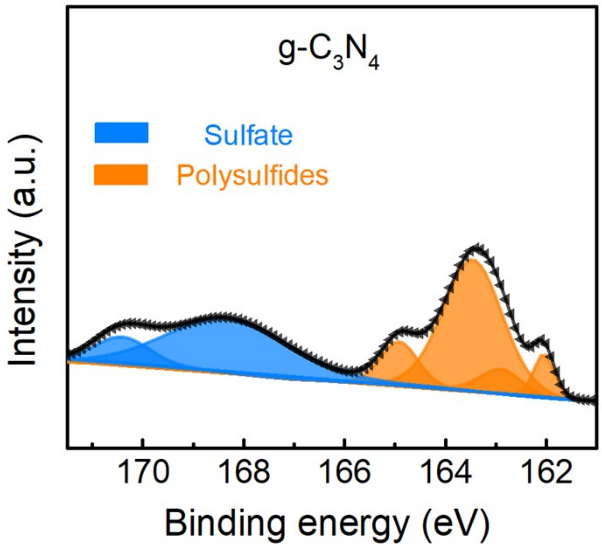

Fig. S10 XPS high-resolution S 2p spectrum of g-C_3N_4 after the adsorption test of Li_2S_6 for 3 h.

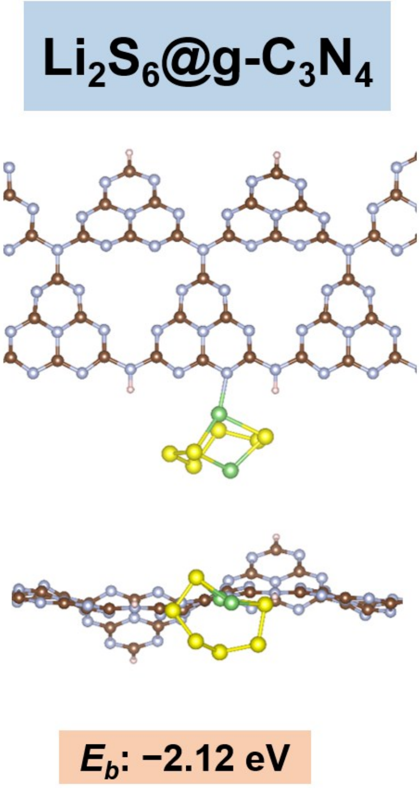

Fig. S11 Binding geometric configurations and binding energies of Li_2S_6 with g-C_3N_4, the strong interaction induces the distortion of C_3N_4 layer. The hydrogen, lithium, carbon, nitrogen, and sulfur atoms are marked with pink, brown, green, blue, and yellow, respectively.

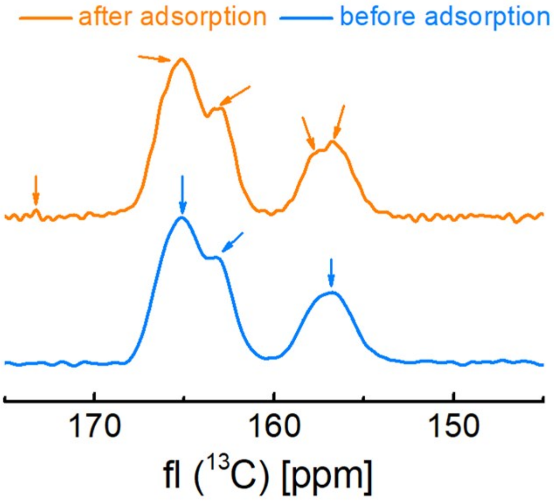

Fig. S12 ^{13}C nuclear magnetic resonance (NMR) spectrum of g-C_3N_4 before and after Li_2S_6 adsorption.

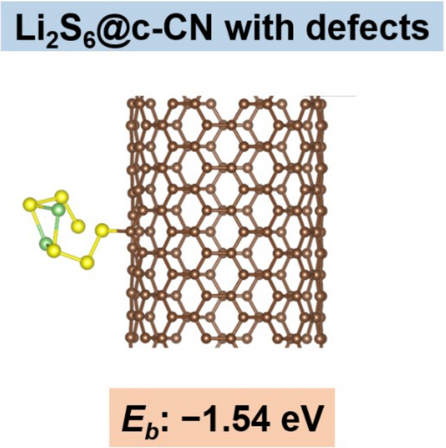

Fig. S13 The geometrical configuration and binding energy of Li_2S_6 with defected c-CN. The lithium, carbon, and sulfur atoms are marked with brown, green, and yellow, respectively.

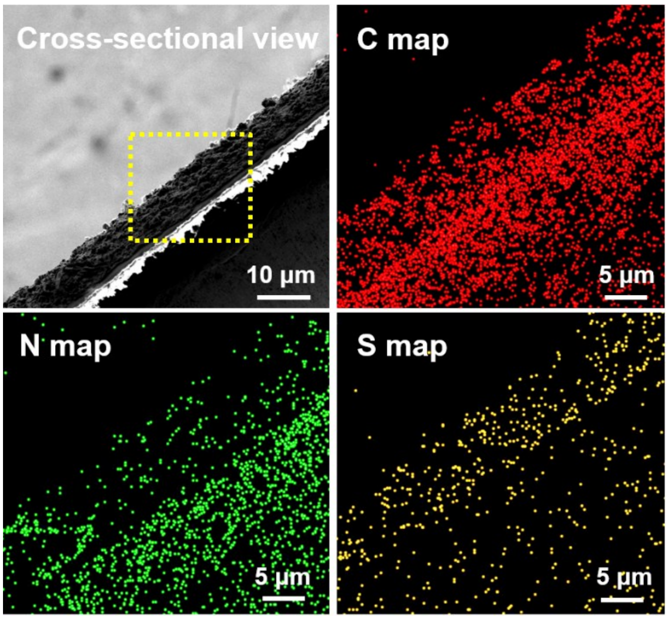

Fig. S14 Cross-sectional SEM and EDS characterization showing the one-side coating of c-CN on the separator after a Li_2S_6 permeation test.

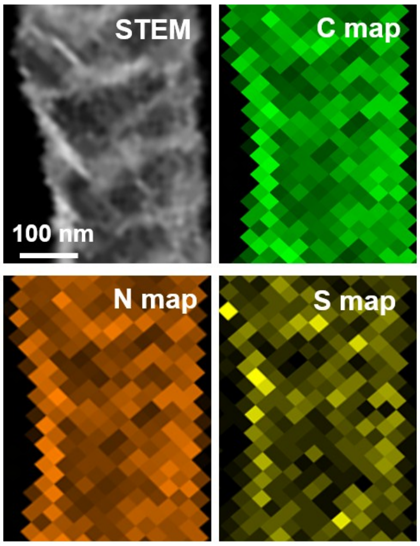

Fig. S15 STEM image and corresponding elemental maps of c-CN after Li_2S_6 adsorption.

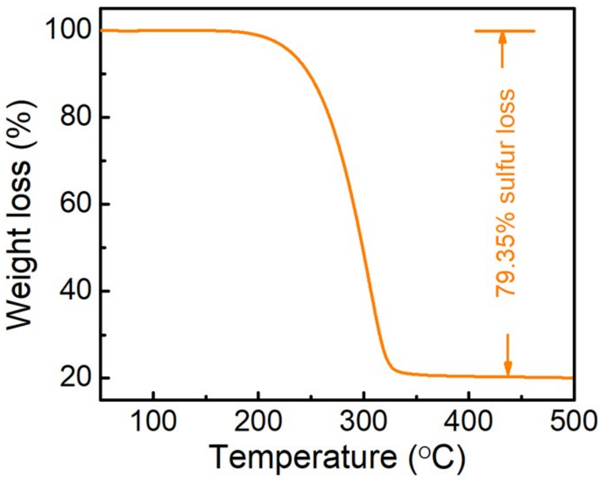

Fig. S16 TGA curve of the sulfur-graphene hybrid, showing a sulfur loss of 79.35%.

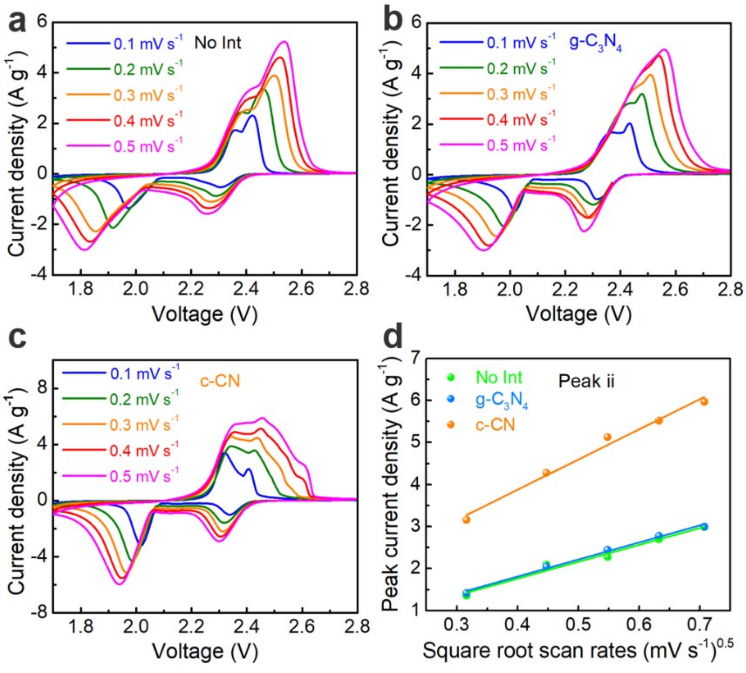

Fig. S17 CV profiles of (a) no interlayer, (b) g-C_3N_4 interlayer, and (c) c-CN interlayer-based cells at various scan rates from 0.1-0.5 mV s^{-1}. (d) Reaction kinetics with respect to the Li^+ ion diffusion properties of peak ii at various scan rates.

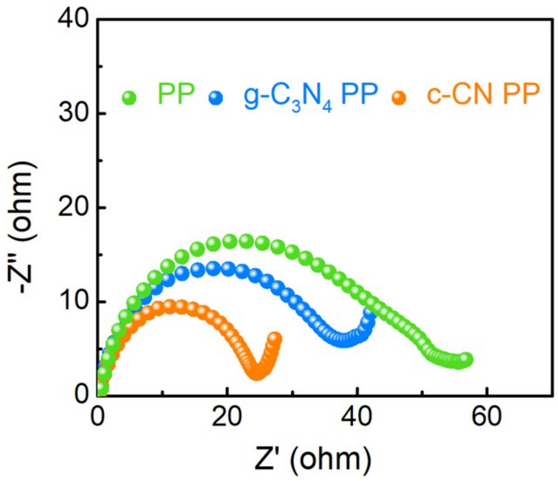

Fig. S18 EIS of the bare PP, g-C_3N_4 PP and c-CN PP based cells.

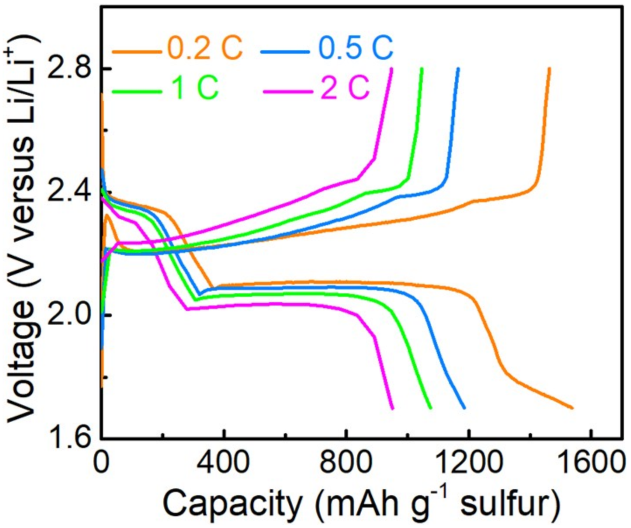

Fig. S19 Galvanostatic charge–discharge curves of c-CN PP based cell at various current densities.

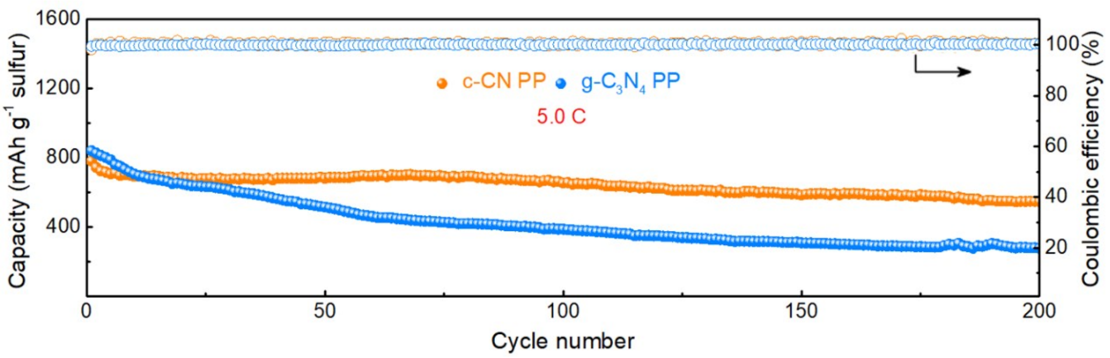

Fig. S20 Cyclic performance at 5.0 C of g-C_3N_4 PP and c-CN PP, respectively.

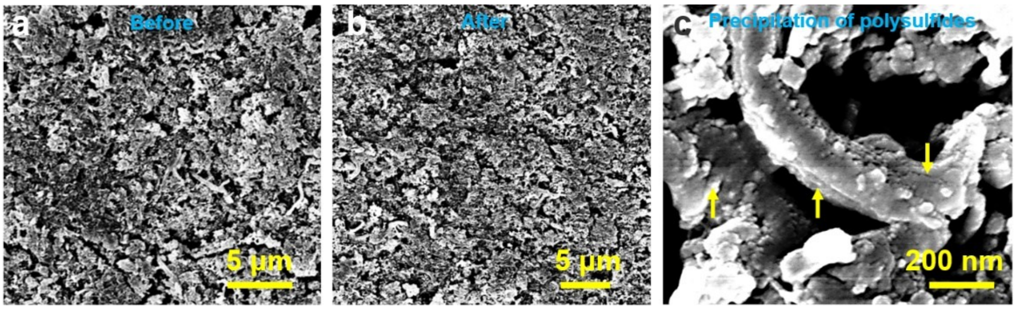

Fig. S21 SEM inspection of the c-CN PP a) before, and b) after 200 cycles at 2.0 C. c) The precipitation of solid short-chain polysulfides on the c-CN after battery cycling.

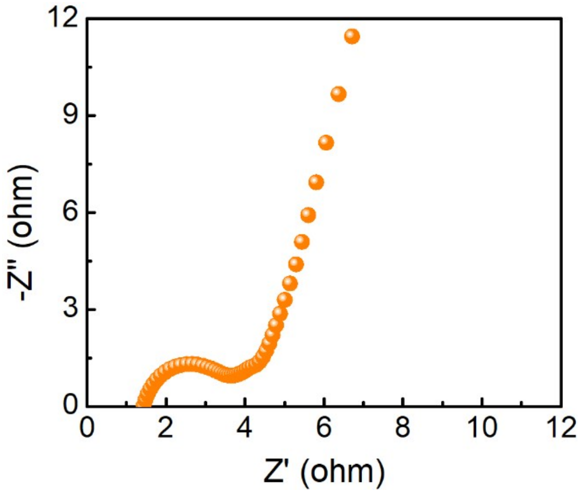

Fig. S22 EIS spectrum of c-CN-derived supercapacitor in a three-electrode configuration.

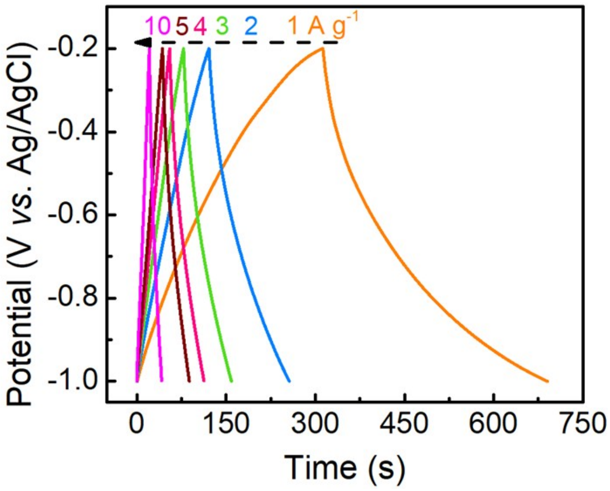

Fig. S23 Galvanostatic charge-discharge curves of c-CN at various current density of 1–10 A g^{-1} in a three-electrode configuration.

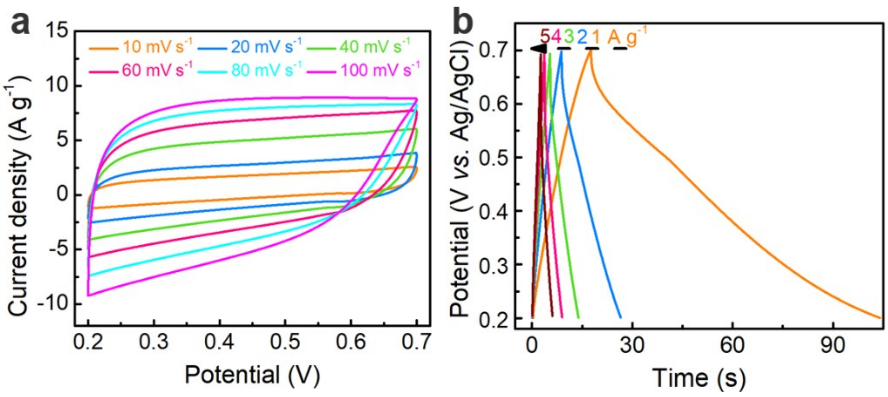

Fig. S24 (a) CV profiles of c-CN-derived SSC at different scan rates of 10–100 mV s^{-1}. (b) Galvanostatic charge-discharge curves of SSC at different current densities of 1–5 A g^{-1}.

Table S1 Comparison of battery performances at high sulfur loading conditions based on various modified-separators between this work and other reported studies.

Coating materials	**Host**	**Loading (mg cm^{-2})**	**S content (wt%)**	**Rate (C)**	**Cycles**	**Initial capacity (mAh cm^{-2})**	**Capacity decay (% per cycle)**	**Ref.**
c-CN	Graphene	3.56	63	1.0	100	2.82	0.32	This work
		5.23	60	0.2	100	5.75	0.21	
		9.80	60	0.2	50	5.77	0.56	
MoS_2-PDDA	Ketjen Black	4.0	60	1.0	100	3.1	0.35	1
PAN@APP	Carbon powders	6.0	70	0.2	50	3.66	0.07	2
N-doped graphene	Graphene	3.8	61	0.3	30	4.45	1.06	3
Co_9S_8	Super P	5.6	70	-	200	5.05	0.08	4
rGO@SL	Carbon powders	3.8	50	0.1	50	2.30	0.34	5
Ce-MOF/CNT	Ketjen Black	2.5	-	1.0	800	2.55	0.02	6
LDH/NG	CNTs	4.3	63	0.5	100	4.64	0.26	7
$Ni_3(HITP)_2$ or ZIF-8	Carbon black	3.5	64	1.0	500	2.98	0.03	8

Supporting references:

1 J. Y. Wu, H. X. Zeng, X. W. Li, X. Xiang, Y. G. Liao, Z. G. Xue, Y. S. Ye and X. L. Xie, *Adv. Energy Mater.*, 2018, **8**, 1802430.

2 T. Y. Lei, W. Chen, Y. Hu, W. Q. Lv, X. X. Lv, Y. C. Yan, J. W. Huang, Y. Jiao, J. W. Chu, C. Y. Yan, C. Y. Wu, Q. Li, W. D. He and J. Xiong, *Adv. Energy Mater.*, 2018, **8**, 1802441.

3 Q. C. Li, Y. Z. Song, R. Z. Xu, L. Zhang, J. Gao, Z. Xia, Z. N. Tian, N. Wei., M. H. Rümmeli, X. L. Zou, J. Y. Sun and Z. F. Liu, *ACS Nano*, 2018, **12**, 10240-10250.

4 J. R. He, Y. F. Chen and A. Manthiram, *Energy Environ. Sci.*, 2018, **11**, 2560-2568.

5 T. Y. Lei, W. Chen, W. Q. Lv, J. W. Huang, J. Zhu, J. W. Chu, C. Y. Yan, C. Y. Wu, Y. H. Yan, W. D. He, J. Xiong, Y. R. Li, C. L. Yan, J. B. Goodenough and X. F. Duan, *Joule*, 2018, **2**, 2091-2104.

6 X. J. Hong, C. L. Song, Y. Yang, H. C. Tang, G. H. Li, Y. P. Cai and H. X. Wang, *ACS Nano*, 2019, **13**, 1923-1931.

7 H. J. Peng, Z. W. Zhang, J. Q. Huang, G. Zhang, J. Xie, W. T. Xu, J. L. Shi, X. Chen, X. B. Cheng and Q. Zhang, *Adv. Mater.*, 2016, **28**, 9551-9558.

8 Y. Zang, F. Pei, J. H. Huang, Z. H. Fu, G. Xu and X. L. Fang, *Adv. Energy Mater.*, 2018, **8**, 1802052.